C. R. Physique 17 (2016) 995–1002

Contents lists available at ScienceDirect

Comptes Rendus Physique

www.sciencedirect.com

Probing matter with electromagnetic waves / Sonder la matière par les ondes électromagnétiques

Scattering properties of a stratified air/snow/sea ice medium. Small slope approximation

Diffusion par un milieu stratifié air/neige/mer glacée. Modèle des faibles pentes

Richard Dusséaux [a,*], Saddek Afifi [b], Monique Dechambre [a]

[a] *Université de Versailles Saint-Quentin-en-Yvelines, LATMOS/IPSL, 10–12, av. de l'Europe, 78140 Vélizy, France*
[b] *Département d'Électronique, Université Badji Mokhtar Annaba, P.O. Box 12, 23000 Annaba, Algeria*

ARTICLE INFO

Article history:
Available online 10 August 2016

Keywords:
Small slope approximation
Layered medium
Scattered intensity

Mots-clés :
Modèle des faibles pentes
Milieu multicouches
Intensité diffractée

ABSTRACT

The sea-ice thickness, a key parameter in Arctic studies, is derived from radar altimeter height measurements of the freeboard, taking into account not only snow load, but also the penetration depth of the electromagnetic waves inside the snow—this is the not generally the case. Within the framework of the small slope approximation method, we study in Ku-band ($f = 13$ GHz, $\lambda = 2.31$ cm in the air) the electromagnetic signature of an air/snow/sea ice rough layered medium. The snow is inhomogeneous and is represented as a stack of several layers with different relative permittivities. We show that the electromagnetic response is very sensitive to the isotropy factor of the air/snow interface and to the cross-correlation parameters of interfaces.

RÉSUMÉ

L'épaisseur des glaces de mer est un paramètre clé pour l'étude du fonctionnement de la zone arctique. Cette grandeur est obtenue à l'aide de mesures faites depuis un altimètre radar spatial du bord franc de la banquise. Mais ceci suppose que non seulement la charge de neige qui recouvre la glace de mer, mais aussi la distance de pénétration de l'onde dans le milieu soient connues, ce qui n'est en général pas le cas. Dans ce contexte, nous étudions à l'aide de la méthode des faibles pentes la signature radar en bande Ku ($f = 13$ GHz, $\lambda = 2.31$ cm dans l'air) d'une mer gelée enneigée sous la forme d'une configuration air/neige/glace/mer. La couche de neige est inhomogène et représentée comme un empilement de plusieurs couches ayant des permittivités relatives différentes. Nous mettons en évidence l'influence combinée sur la signature radar du facteur d'isotropie de l'interface air/neige et des facteurs de corrélation entre les différentes interfaces.

* Corresponding author.
E-mail address: Richard.dusseaux@latmos.ipsl.fr (R. Dusséaux).

http://dx.doi.org/10.1016/j.crhy.2016.07.017

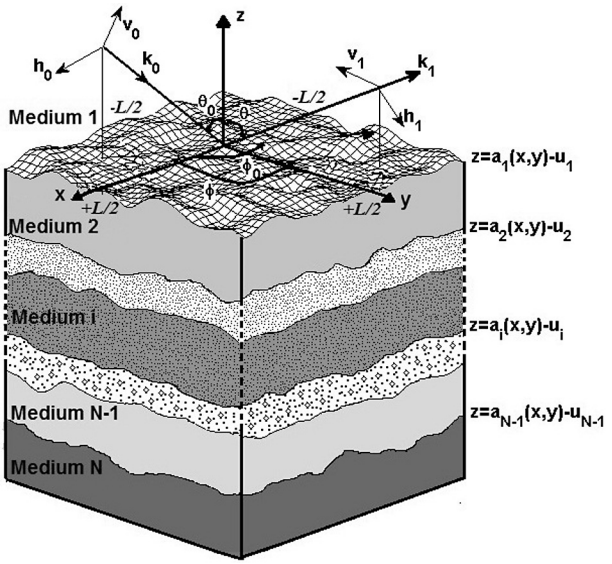

Fig. 1. Structure with several 2D rough interfaces.

1. Introduction

Remote sensing of the arctic sea ice thickness is one of the main objectives of the CRYOSAT II mission, carrying onboard a Ku-band radar altimeter [1]. On the one hand, the sea ice thickness is derived from the freeboard measurement of the ice, based on isostasy and assuming that the densities of the water and the ice as well as the snow are known [2]. On the other hand, even if the snow load is known, the penetration of the electromagnetic waves into the snow strongly depends on the electrical and geophysical characteristics of the snow layer (density, temperature, permittivity, roughness). The remote sensing of the snow layer thickness remains a real challenge and, in this specific context, the study of the scattering properties of electromagnetic waves from a stack of random rough interfaces by means of analytical models [3,4] or numerical models [5,6] is of great interest.

The small slope approximation method (SSA) is an analytical model that has been extensively used for studying the radar signatures of the ocean surfaces [7,8] as well as the scattering diagram of industrial surfaces [9]. This model is attractive because its domain of validity includes the small perturbation model (SPM), valid for a roughness smaller than the incident wavelength [10], and the Kirchhoff model, valid for surfaces with a radius of curvature greater than the wavelength [11].

The SSA method at the first order provides the scattering amplitude in the form of an integral where the integrant depends on the kernel of the SPM method at the first order. Therefore the SSA method gives the results of SPM when the roughness becomes small. Knowing the first-order electromagnetic kernels of SPM, it is then possible to derive the expression of the amplitude of the scattered wave within the framework of the first-order SSA method. In [12], the SSA method is implemented for a stack of two interfaces. In [13] and [14], starting from the knowledge of the first-order kernels of SPM, the first-order SSA method has been extended to a stratified medium with an arbitrary number of interfaces. The different rough interfaces separating homogeneous layers may be correlated or not, isotropic or not.

In this paper, we present a study of the radar signature in the Ku-band of a sea ice medium covered with snow, in the air/snow/ice/sea configuration [15], by means of the first-order SSA method. The snow load is inhomogeneous and represented by a stack of several layers with different relative permittivities [16]. We show that the electromagnetic response is very sensitive to the isotropy factor of the air/snow interface and to the correlations between the different interfaces.

2. Description of the medium

The stratified medium is a stack of N layers (Fig. 1). The interfaces are randomly deformed over an area $L \times L$. For the study, the length L is extended to infinity. The interfaces i and $i+1$ are separated by a layer, spatially homogeneous and isotropic, with thickness $d_i = u_{i+1} - u_i$ (with $u_1 = 0$). The functions $a_i(x, y)$ describing the interfaces i (with $1 \leq i \leq N-1$) are Gaussian zero mean random processes, stationary to the second order. For the numerical applications, the autocorrelation functions $R_{ii}(x, y)$ and the cross-correlation functions $R_{i,j\neq i}(x, y)$ are assumed Gaussian and defined as follows [17,18]:

$$R_{ij}(x, y) = 2q_{ij}\sigma_i\sigma_j \sqrt{\frac{l_{xi}l_{xj}l_{yi}l_{yj}}{(l_{xi}^2 + l_{xj}^2)(l_{yi}^2 + l_{yj}^2)}} \exp\left(-\frac{2x^2}{l_{xi}^2 + l_{xj}^2} - \frac{2y^2}{l_{yi}^2 + l_{yj}^2}\right) \tag{1}$$

Table 1
Complex relative permittivity values and layer thickness values.

Medium	Relative permittivity	Thickness (cm)
1 – Air	1	–
2 – Snow	1.58 – 0.0587j	3.10
3 – Snow	1.82 – 0.1034j	2.85
4 – Snow	1.57 – 0.0428j	2.80
5 – Snow	2.81 – 0.0005j	3.20
6 – Snow	1.30 – 0.0435j	3.00
7 – Snow	2.81 – 0.0001j	2.90
8 – Snow	1.32 – 0.0001j	3.15
9 – Sea ice	4.4 – 0.38j	80
10 – Seawater	31 – 39j	–

Table 2
RMS heights and correlation lengths of the interfaces – limit angle of validity of SSA.

Interfaces	σ_i (cm)	(l_{xi}, l_{yi}) (cm)	θ_{lim} in degrees
1 – Air/Snow	0.24	(1.20;1.20) or (1.20;2.40)	79 or 84
2 – Snow/Snow	0.245	(1.21;1.21)	79
3 – Snow/Snow	0.235	(1.19;1.19)	79
4 – Snow/Snow	0.24	(1.20;1.20)	79
5 – Snow/Snow	0.25	(1.10;1.10)	77
6 – Snow/Snow	0.23	(1.13;1.13)	78
7 – Snow/Snow	0.24	(1.20;1.20)	79
9 – Snow/Sea ice	0.28	(1.80;1.80)	81
10 – Sea ice/Seawater	0.9	(24;24)	88

σ_i is the RMS height of the interface i. l_{xi} and l_{yi} represent the correlation lengths in both Ox and Oy directions. The interface is isotropic if $l_{xi} = l_{yi}$ and anisotropic if $l_{xi} \neq l_{yi}$. The isotropy factor is defined as the ratio $r_i = \frac{\min(l_{xi}, l_{yi})}{\max(l_{xi}, l_{yi})}$. q_{ij} is the mixing parameter with $|q_{i,j\neq i}| \leq 1$ and $q_{ii} = 1$ [19]. If $q_{i,j\neq i} = 0$, the interfaces i and j are uncorrelated. They are fully correlated when $l_{xi} = l_{xj}$, $l_{yi} = l_{yj}$ and $q_{ij} = \pm 1$. They are partially correlated in other cases [18,19]. The spectrum $\hat{R}_{ii}(\alpha, \beta)$ of the interface i and the cross-spectrum $\hat{R}_{i,j\neq i}(\alpha, \beta)$ between the interfaces i and j correspond to the Fourier Transforms (FT) of $R_{ii}(x, y)$ and $R_{ij}(x, y)$ and they are also Gaussian functions.

In the case of our study, we consider a standard configuration proposed by Tonboe et al. in [16]: a stack of seven snow layers, laying on a sea ice layer, and a sea water layer. The stratified medium is illustrated by a monochromatic plane wave ($f = 13$ GHz, $\lambda = 2.31$ cm in the air). The complex permittivity values at 13 GHz are given in Table 1 [16]. The RMS heights and the correlation lengths of the rough interfaces are given in Table 2 and proposed in [20]. For the study, the anisotropy only concerns the air/snow interface (for instance, this anisotropy can be caused by wind). Insofar as the snow deposit on a surface depends on the geometry of this surface, we can think that the interfaces separating the different layers are correlated. For the study, we compare the two extreme case for which the interfaces are uncorrelated ($q_{i,j\neq i} = 0$ and $q_{ii} = 1$) and highly correlated ($q_{ij} = 1$), respectively.

3. Coherent and incoherent intensities

The wave vector $\mathbf{k}_0$ of the incident plane wave is defined by its zenith angle θ_0 and its azimuth angle ϕ_0. Its components $(\alpha_0, \beta_0, -\gamma_0)$ in a Cartesian coordinate system are given by:

$$\alpha_0 = k_1 \sin\theta_0 \cos\phi_0; \qquad \beta_0 = k_1 \sin\theta_0 \sin\phi_0; \qquad \gamma_0 = k_1 \cos\theta_0 \tag{2}$$

k_1 is the wave number in the air. The incident electric and magnetic field vectors are defined as follows:

$$\mathbf{E}_0 = (A_{0(h)}\mathbf{h}_0 + A_{0(v)}\mathbf{v}_0)\exp(-\mathrm{j}\mathbf{k}_0 \cdot \mathbf{r}) \tag{3}$$

$$\mathbf{H}_0 = \frac{1}{Z_1}(-A_{0(h)}\mathbf{v}_0 + A_{0(v)}\mathbf{h}_0)\exp(-\mathrm{j}\mathbf{k}_0 \cdot \mathbf{r}) \tag{4}$$

where $\mathbf{r}(x, y, z)$ is the position vector in the Cartesian coordinate system, $\mathbf{h}_0$ and $\mathbf{v}_0$ are the polarization vectors [21]. For an incident wave with a horizontal polarization, $A_{0(h)} = 1$ and $A_{0(v)} = 0$. For the vertical polarization, $A_{0(h)} = 0$ et $A_{0(v)} = 1$. The stratified medium illuminated by an (a)-polarized incident plane wave generates a scattered wave with a co-polarized component (aa) and a cross-polarized component (ba). In the far-field region above the surface, under the observation direction defined by the zenith angle θ and the azimuth angle ϕ, the coherent intensity $I_{c,(ba)}(\theta, \phi)$ is proportional to the square modulus of the statistical average of the complex scattered amplitude $A_{1(aa)}(\theta, \phi)$ [21]:

$$I_{c,(ba)}(\theta,\phi)=\lim_{L\to+\infty}\frac{|\langle A_{1(ba)}(\theta,\phi)\rangle|^2\cos^2\theta}{\cos\theta_0\lambda^2L^2|A_{0(a)}|^2} \tag{5}$$

The brackets $\langle\ \rangle$ stand for a statistical average. The statistical average of scattering intensity (i.e. the bi-static scattering coefficient) is proportional to the statistical average of the square modulus of the scattered amplitude:

$$I_{(ba)}(\theta,\phi)=\lim_{L\to+\infty}\frac{\langle|A_{1(ba)}(\theta,\phi)|^2\rangle\cos^2\theta}{\cos\theta_0\lambda^2L^2|A_{0(a)}|^2} \tag{6}$$

The incoherent intensity $I_{f,(ba)}(\theta,\phi)$ is the difference between (5) and (6) [21]:

$$I_{f,(ba)}(\theta,\phi)=I_{(ba)}(\theta,\phi)-I_{c,(ba)}(\theta,\phi) \tag{7}$$

For a stratified medium with an arbitrary number of interfaces, the scattered amplitudes $A_{1(ba)}(\theta,\phi)$ can be evaluated by means of a first-order perturbation method. The electromagnetic field in each layer is represented by a continuous spectrum of plane waves, the amplitudes of which are found by matching the boundary value problem at both interfaces. The perturbation method consists of representing the scattering amplitudes and wave functions by expansions in entire series. In [13,14], we obtain a closed-form first-order solution for an arbitrary number of rough interfaces. The scattering amplitudes in each medium are derived from recurrence relations. In the air, the scattering amplitude $A_{1(ba)}(\theta,\varphi)$ is given by:

$$A^{(\mathrm{SPM})}_{1(ba)}(\theta,\phi)=4\pi^2A^{(0)}_{1(a)}(\alpha_0,\beta_0)\delta(\zeta)\delta(\xi)+A^{(1)}_{1(ba)}(\alpha,\beta) \tag{8}$$

where $\zeta=\alpha-\alpha_0$; $\xi=\beta-\beta_0$, $\alpha=k_1\sin\theta\cos\phi$, $\beta=k_1\sin\theta\sin\phi$, δ denotes the Dirac distribution. The zeroth-order amplitude $A^{(0)}_{1(a)}$ is the reflecting Fresnel coefficient for a planar structure. The zeroth-order solution is in the specular direction and is not depolarized. The first-order solution $A^{(1)}_{1(ba)}$ can be written in the following form:

$$A^{(1)}_{1(ba)}=\sum_{i=1}^{N-1}K_{i(ba)}(\alpha,\beta)\hat{a}_i(\zeta,\xi) \tag{9}$$

$\hat{a}_i(\alpha,\beta)$ is the Fourier transform of the function $a_i(x,y)$ describing the interface i. The factors $K_{i(ba)}(\alpha,\beta)$ are given by recurrent formulas [13,14]. They depend on the relative permittivities and the thicknesses of the different layers, and on the zenith and azimuth angles of incident and scattered waves. The coherent and incoherent intensities can be derived from (5) and (6) by using the small perturbations method:

$$I^{(\mathrm{SPM})}_{c,(a)}(\theta,\phi)=\frac{\cos\theta_0}{\lambda^2}\left|A^{(0)}_{1(a)}(\alpha_0,\beta_0)\right|^2 4\pi^2\delta(\xi)\delta(\zeta) \tag{10}$$

$$I^{\mathrm{SPM}}_{f(ba)}(\theta,\phi)=\frac{\cos^2\theta}{\lambda^2\cos\theta_0}\left\{\sum_{i=1}^{N-1}|K_{i(ba)}|^2\hat{R}_{ii}(\zeta,\xi)+\sum_{i=1}^{N-1}\sum_{\substack{j=1\\j\neq i}}^{N-1}\mathrm{Re}\left[K_{i(ba)}K^*_{j(ba)}\hat{R}_{ij}(\zeta,\xi)\right]\right\} \tag{11}$$

The coherent intensity is in the specular direction and the incoherent intensity depends on the spectra of the different interfaces and on their cross-spectra.

In [13] and [14], from the first-order kernels of SPM, the first-order SSA is extended for a stratified medium with an arbitrary number of interfaces. It is demonstrated that the complex scattering amplitude can be written as:

$$A^{(\mathrm{SSA})}_{1(ba)}=A_{0(a)}\sum_{i=1}^{N-1}\frac{K_{i(ba)}}{\mathrm{j}(\gamma_1+\gamma_0)}\int_{-\infty}^{+\infty}\int_{-\infty}^{+\infty}\exp(\mathrm{j}\zeta x)\exp(\mathrm{j}\xi y)\exp\left[\mathrm{j}(\gamma_1+\gamma_0)a_i(x,y)\right]\mathrm{d}x\,\mathrm{d}y \tag{12}$$

where $\gamma_1=k_1\cos\theta$. The solution (12) is consistent with (8) for small roughness interfaces if:

$$A^{(0)}_{1(a)}=\begin{cases}\sum_{i=1}^{N-1}\frac{K_{i(aa)}(\alpha_0,\beta_0)}{j2\gamma_0} & \text{if } (a)=(b)\\ 0 & \text{if } (a)\neq(b)\end{cases} \tag{13}$$

We can derive from (5), (7) and (12) the coherent and incoherent intensities, and we find:

$$I^{\mathrm{SSA}}_{c,(ba)}(\theta,\phi)=\frac{4\pi^2\delta(\zeta)\delta(\xi)}{4\lambda^2k_1^2\cos\theta_0}\left|\sum_{i=1}^{N-1}K_{i(ba)}(\alpha_0,\beta_0)\exp\left(-2\gamma_0^2\sigma_i^2\right)\right|^2 \tag{14}$$

$$I^{\mathrm{SSA}}_{f,(ba)}(\theta,\phi)=\frac{\gamma_1^2}{4\pi^2\cos\theta_0(\gamma_1+\gamma_0)^2}\sum_{i=1}^{N-1}\sum_{j=1}^{N-1}K_{i,(ba)}K^*_{j,(ba)}\exp\left[-\frac{\sigma_i^2+\sigma_j^2}{2}(\gamma_1+\gamma_0)^2\right]P_{ij} \tag{15}$$

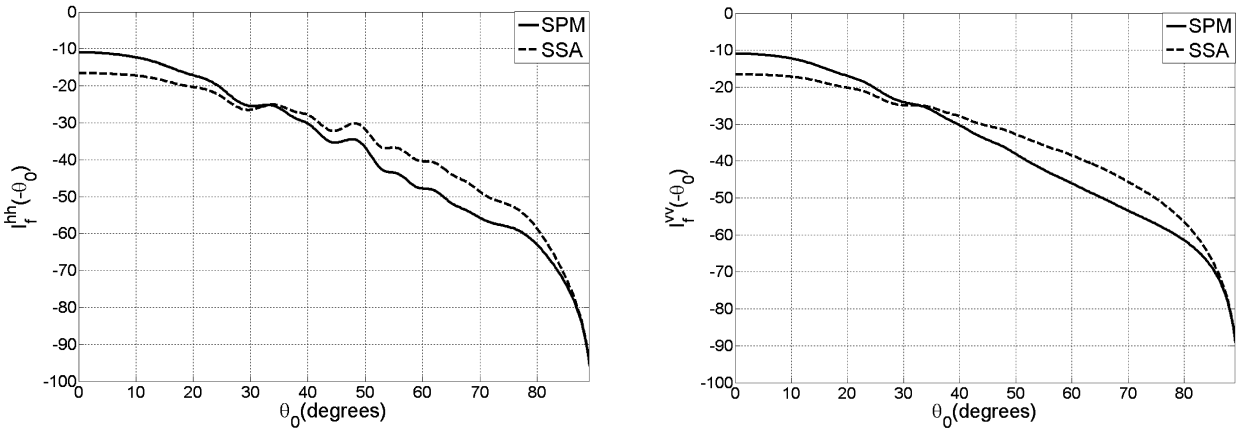

Fig. 2. Backscattered incoherent intensities for isotropic and uncorrelated interfaces. Left: (hh)-polarization, right: (vv)-polarization.

with

$$P_{ij} = \sum_{q=1}^{+\infty} \frac{(\gamma_1 + \gamma_0)^{2q}}{q!} \mathrm{FT}\left[R_{ij}^q(x, y)\right](\zeta, \xi) \tag{16}$$

where the letters FT designate the Fourier Transform. The coherent intensity $I_{c,(ba)}^{\mathrm{SSA}}(\theta, \phi)$ is in the specular direction. It depends on the RMS heights, but does not depend on the spectra and the cross-spectra. As shown in (15) and (16), the incoherent intensity $I_{f,(ba)}^{\mathrm{SSA}}(\theta, \phi)$ depends on the Fourier Transforms of the functions $R_{ij}(x)$ at the power q. For small roughness, the formula (15) developed at the second order leads to the incoherent intensity obtained in the SPM case (12). Because $K_{i(hv)} = K_{i(vh)} = 0$, there is no depolarization in the incidence plane and the cross-polarized incoherent intensities derived from the first-order SSA are equal to zero in the plane $\phi = \phi_0$.

4. Numerical simulations

Fig. 2 shows the backscattered incoherent intensity as a function of the incidence angle for isotropic and uncorrelated interfaces. For $0 \leq \theta_0 \leq 34°$, the SPM method overestimates the SSA method with a maximum difference of 6.4 dB. For $\theta_0 > 34°$, the SPM method leads to smaller values than those obtained with the SSA method, with a maximum difference of 7.6 dB.

For a randomly rough surface separating the air from a homogeneous medium, the validity domain of the small-slope approximation is given as follows [9]:

$$\frac{\sigma}{l} < \min(1/\tan\theta_0, 1/\tan\theta) \tag{17}$$

The limiting values for the incidence angle and the observation angle are shown in the fourth column of Table 2. For each interface taken separately, the angular range of validity is broad. The applicability domain of the SSA method for multilayered medium has not been clearly determined. Nevertheless, in [13], for configurations with three interfaces having similar root-mean square slopes, it is shown that the validity domain of the SSA method is twice that of the SPM method in terms of roughness. Taking into account the differences between the two methods (Fig. 2) and according to the limiting values given in Table 2 and with our previous work [13], the SSA method is chosen now in order to investigate the combined influence of the isotropy factor of the first interface and the cross-correlations between interfaces upon the incoherent intensity.

Fig. 3 gives the backscattered incoherent intensity as a function of the incidence angle θ_0 in the incidence plane $\phi = \phi_0 = 0°$. For uncorrelated interfaces, $q_{i,j\neq i} = 0$ and $q_{ii} = 1$. For correlated interfaces, $q_{ij} = 1$. In the anisotropic case, $l_{y1} = 2l_{x1}$ and the isotropy factor of the first interface is equal to 1/2. For interfaces, correlated or not, the anisotropy of the first interface leads to an increase in the backscattering coefficient in the incidence plane.

In the case of a first snow layer, isotropic or not, the correlations give rise to significant oscillations (due to the terms $K_{i,(aa)}K_{j,(aa)}^{*}P_{ij}$ in (15)). Because of these oscillations, there exist several incidence angles for which different configurations (isotropic or anisotropic/uncorrelated and anisotropic or isotropic/correlated) have the same backscattering coefficient. Beyond 85°, the backscattered intensity is almost the same for the four configurations.

In the case of isotropic configurations, the backscattered incoherent intensity does not depend on the azimuth angle. It is no longer the case for the anisotropic configurations. Fig. 4 gives the backscattered intensity as a function of the incidence angle θ_0 in the Oxz plane (i.e. for $\phi = \phi_0 = 0°$) and in the Oyz plane (i.e. for $\phi = \phi_0 = 90°$) for anisotropic configurations.

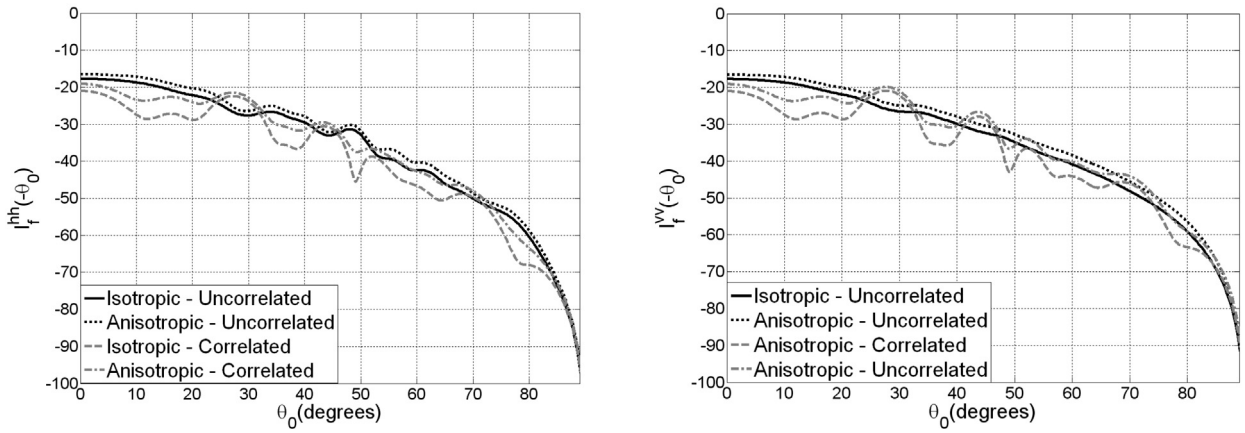

Fig. 3. Backscattered incoherent intensities for isotropic/anisotropic/correlated/uncorrelated configurations. Left: (hh)-polarization, right: (vv)-polarization. $\phi = \phi_0 = 0°$.

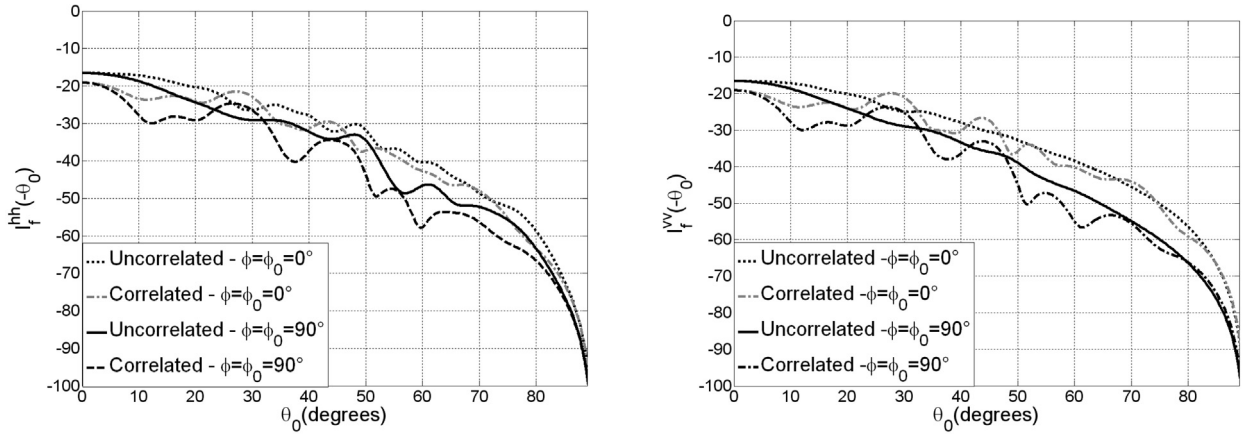

Fig. 4. Backscattered incoherent intensities in the incidence planes Oxz $(\phi = \phi_0 = 0°)$ and Oyz $(\phi = \phi_0 = 90°)$ for anisotropic configurations. Left: (hh)-polarization, right: (vv)-polarization.

For a given correlation, the backscattered incoherent intensity in the Oxz plane is greater than the one in the perpendicular plane Oyz. The differences deduced from the curves can be large. The maximum difference is 15 dB for the (hh)-polarization and 16.3 dB for the (vv)-polarization.

Fig. 5 gives the incoherent intensity as a function of the observation angle θ for configurations illuminated under normal incidence ($\theta_0 = 0°$, $\phi = \phi_0 = 0°$). For correlated or uncorrelated interfaces as well, the anisotropy of the first interface generates an increase in the intensity. For a first interface, isotropic or anisotropic as well, the correlations generate important oscillations (due to the terms $K_{i,(aa)} K^*_{j,(aa)} P_{ij}$ in (15)). The maximum difference between the two isotropic configurations reaches the value 15.5 dB for (hh)-polarization. The maximum difference is equal to the value 16.8 dB for (vv)-polarization. Because of these oscillations, there exist several observation angles for which different configurations (isotropic or anisotropic/uncorrelated and anisotropic or isotropic/correlated) give the same value of the incoherent intensity.

Fig. 6 shows the incoherent intensity as a function of the observation angle θ for three incidence planes under normal incidence, i.e. $\varphi = \varphi_0$ with $\varphi = 0°$, $45°$ and $90°$. The interfaces are uncorrelated and the first snow layer is anisotropic. For anisotropic interfaces and a given observation angle, the value of the incoherent intensity depends on the incidence plane. The values of the intensity are close in the plane $\phi = \phi_0 = 45°$ and $\phi = \phi_0 = 90°$. The differences with the values obtained in the plane $\phi = \phi_0 = 0°$ can be important and reach 5 dB.

5. Conclusion

In this paper, we have investigated the radar signature in the Ku band of a natural stratified structure with a layer of sea ice covered with seven snow layers. This study was conducted in the context of the remote sensing of sea ice thickness by means of radar altimeters, for which the snow load over sea ice is a source of measurement error. We have studied the influence of the isotropy factor of the air/snow interface and the cross-correlations between the interfaces upon

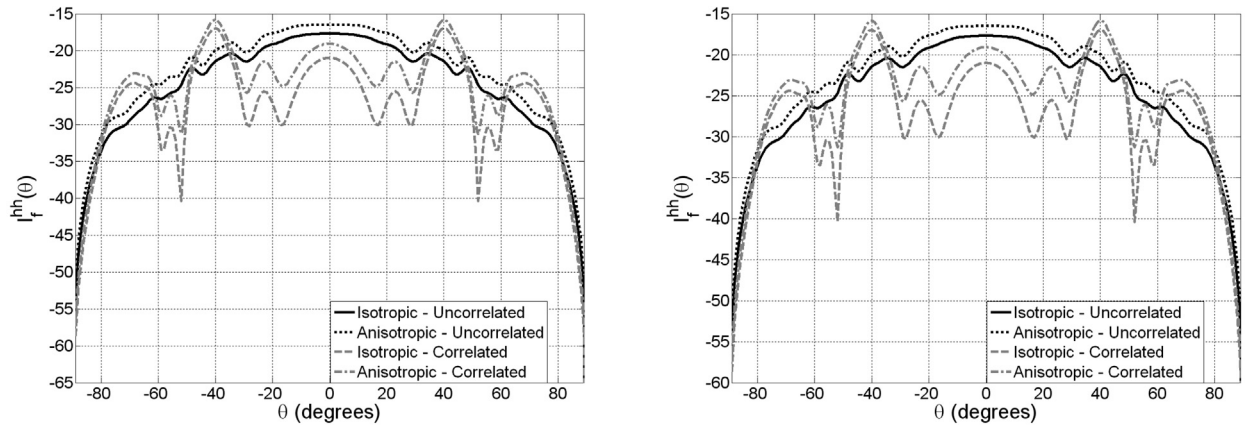

Fig. 5. Incoherent intensities for isotropic/anisotropic/correlated/uncorrelated configurations under normal incidence. Left: (hh)-polarization, right: (vv)-polarization. $\phi = \phi_0 = 0°$.

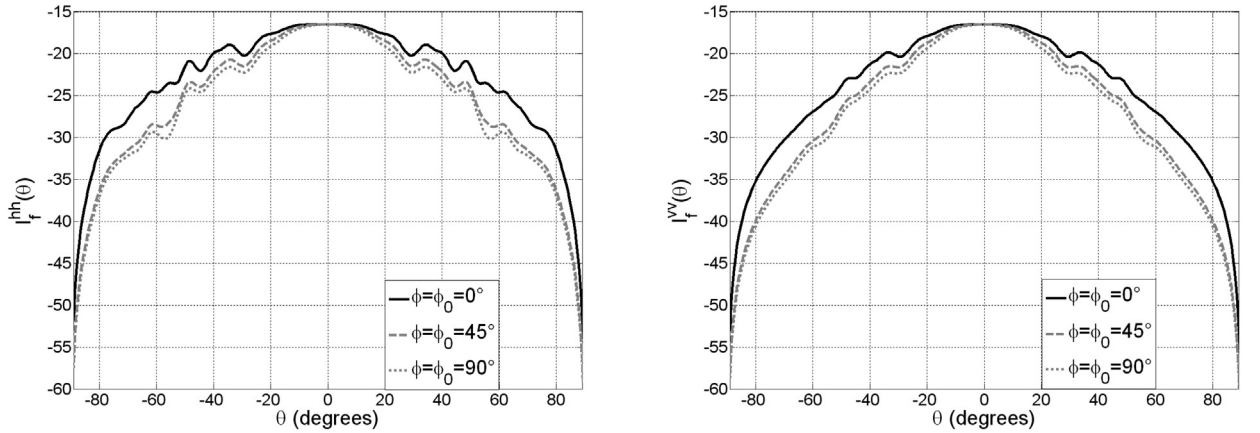

Fig. 6. Incoherent intensities for anisotropic/uncorrelated configurations under normal incidence in three incidence planes. Left: (hh)-polarization, right: (vv)-polarization.

the backscattering coefficient and the incoherent intensity by means of the SSA method. For correlated or uncorrelated interfaces, the first interface anisotropy leads to an increase in the backscattering coefficient, and, in a general manner, to an increase in the incoherent intensity. The cross-correlations give rise to oscillations of several dB. As a result, there exist several incidence angles for which different configurations (isotropic or anisotropic/uncorrelated and anisotropic or isotropic/correlated) give the same backscattering coefficient. Beyond 85°, the backscattered intensity weakly depends on the isotropy factor and the correlation parameters. For anisotropic configurations, the backscattered incoherent intensity depends on the incidence plane. For two perpendicular incidence planes, differences of 15 to 16 dB are observed. As well, we have noted that for a given incidence, there exist several observation angles for which configurations with different isotropy factors and correlation coefficients give rise to the same value of the incoherent intensity. For an anisotropic air/snow interface, the incoherent intensity in terms of the zenith observation angle changes from one incidence plane from another.

All these different simulations have shown that the electromagnetic response of a layered medium is very sensitive to the isotropy factors as well as to the cross-correlations between the interfaces. These results must be taken into account for analysis purposes of the electromagnetic signature of an air/snow/ice/sea structure and impose a fine description of the medium, knowing that the snow surface isotropy or the correlations between snow layers have not been really investigated until now. This is an important result to be kept in mind when attempting a signal inversion.

Acknowledgements

The authors thank the “Programme national de télédétection spatiale”, which has supported this research.

References

[1] D.J. Wingham, C.R. Francis, S. Baker, C. Bouzinac, D. Brockley, R. Cullen, P. de Château-Thierry, S.W. Laxon, U. Mallow, C. Mavrocordatos, L. Phalippou, G. Ratier, L. Rey, F. Rostan, P. Viau, D.W. Wallis, CryoSat: a mission to determine the fluctuations in Earth's land and marine ice fields, Adv. Space Res. 37 (2006) 841–871.

[2] T.W.K. Armitage, M.W.J. Davidson, Using the interferometric capabilities of the ESA CryoSat-2 mission to improve the accuracy of sea ice freeboard retrievals, IEEE Trans. Geosci. Remote Sens. 52 (2014) 529–536.

[3] K.M. Golden, D. Borup, M. Cheney, E. Cherkaeva, M.S. Dawson, D. Kung-Hau, A.K. Fung, D. Isaacson, S.A. Johnson, A.K. Jordan, J.A. Kong, R. Kwok, S.V. Nghiem, R.G. Onstott, J. Sylvester, D.P. Winebrenner, I.H.H. Zabel, Inverse electromagnetic scattering models for sea ice, IEEE Trans. Geosci. Remote Sens. 36 (1998) 1675–1704.

[4] A.S. Komarov, L. Shafai, D.G. Barber, Electromagnetic wave scattering from rough boundaries interfacing inhomogeneous media and application to snow-covered sea ice, Prog. Electromagn. Res. 144 (2014) 201–219.

[5] D. Isleifson, I. Jeffrey, L. Shafai, J. LoVetri, D.G. Barber, A Monte Carlo method for simulating scattering from sea ice using FVTD, IEEE Trans. Geosci. Remote Sens. 50 (2012) 2658–2668.

[6] J.P. Samluk, C.A. Geiger, C.J. Weiss, Full-physics 3-D heterogeneous simulations of electromagnetic induction fields on level and deformed sea ice, Ann. Glaciol. 56 (2015) 405–414.

[7] A.G. Voronovich, Wave Scattering from Rough Surfaces, Springer, Berlin, 1994.

[8] A.G. Voronovich, V.U. Zavorotny, Theoretical model for scattering of radar signals in Ku- and C-bands from a Rough Sea Surface with breaking waves, Waves Random Media 11 (2001) 247–269.

[9] G. Berginc, Small-slope approximation method: a further study of vector wave scattering from two dimensional surfaces and comparison with experimental data, Prog. Electromagn. Res. 37 (2003) 51–87.

[10] J.A. Ogilvy, Theory of Wave Scattering from Random Rough Surfaces, Adam Hilger, Bristol, 1991.

[11] P. Beckmann, A. Spizzichino, The Scattering of Electromagnetic Waves from Rough Surfaces, Pergamon Press, Oxford, UK, 1963.

[12] C. Berginc, C. Bourrely, The small-slope approximation method applied to a three-dimensional slab with rough boundaries, Prog. Electromagn. Res. 73 (2007) 131–211.

[13] A. Berrouk, R. Dusséaux, S. Afifi, Electromagnetic wave scattering from rough layered interfaces: analysis with the small perturbation method and the small slope approximation, Prog. Electromagn. Res. B 57 (2014) 177–190.

[14] S. Afifi, R. Dusséaux, A. Berrouk, Electromagnetic wave scattering from 3D layered structures with randomly rough interfaces: analysis with the small perturbation method and the small slope approximation, IEEE Trans. Antennas Propag. 62 (10) (2014) 5200–5208.

[15] R. Dusséaux, S. Afifi, M. Dechambre, B. Legresy, Simulations of the altimetric signal intensity from 2D layered air/snow/sea-ice rough interfaces, in: 20 Years of Progress in Radar Altimetry, Venice, Italy, ESA SP 710 (2012).

[16] R.T. Tonboe, L.T. Pedersen, C. Haas, Simulation of satellite radar altimeter sea ice thickness retrieval uncertainty, Cryosph. Discuss. 3 (2009) 513–559.

[17] P. Phu, A. Ishimaru, Y. Kuga, Copolarized and cross-polarized enhanced backscattering from two-dimensional very rough surfaces at millimeter wave frequencies, Radio Sci. 29 (5) (1994) 1275–1291.

[18] S. Afifi, R. Dusséaux, On the co-polarized phase difference of rough layered surfaces: formulas derived from the small perturbation method, IEEE Trans. Antennas Propag. 59 (7) (2011) 2607–2618.

[19] S. Afifi, R. Dusséaux, Scattering by anisotropic rough layered 2D interfaces, IEEE Trans. Antennas Propag. 60 (11) (2012) 5315–5328.

[20] Z.A. Hussein, Y. Kuga, A. Ishimaru, S. Jaruwatanadilok, K. Pak, Angular and Frequency Correlation for Sea-Ice Thickness Retrieval, vol. 5, IGARSS, Anchorage, AK, USA, 2004, pp. 3012–3017.

[21] J.A. Kong, K.H. Ding, C.O. Ao, Scattering of Electromagnetic Waves – Numerical Simulations, Wiley–Interscience, New York, 2001.